PCCP

Single site Fe on the (110) surface of γ-Al2O3: Insights from DFT including periodic boundary approach

Journal:	*Physical Chemistry Chemical Physics*
Manuscript ID	CP-ART-11-2020-005718.R2
Article Type:	Paper
Date Submitted by the Author:	10-Feb-2021
Complete List of Authors:	Gu, Jiande; Shanghai Institute of Materia Medica Shanghai Institutes for Biological Sciences, CAS, DDDC Wang, Jing; Jackson State University, Chemistry Leszczynski, Jerzy; Jackson State University, Department of Chemistry

Single site Fe on the (110) surface of γ-Al_2O_3: Insights from DFT including periodic boundary approach

Jiande Gu,[a, b*] Jing Wang,[a] and Jerzy Leszczynski,[a*]

[a]*Interdisciplinary Nanotoxicity Center*
Department of Chemistry
Jackson State University
Jackson, MS 39217 U. S. A.

[b] *Drug Design & Discovery Center*
State Key Laboratory of Drug Research
Shanghai Institute of Materia Medica
Chinese Academy of Sciences
Shanghai 201203 China

[*] Corresponding authors' email address: JG, jiande@icnanotox.org; JL, jerzy@icnanotox.org.

Abstract

Examination of the stable (110) surface of γ-alumina reveals that there are three different type sites available to host single Fe atom. With the carefully calibrated density functional approach (M12-L/SV), three types of Fe single site on the (110) surface of γ-alumina have been investigated under the periodic boundary conditions. The most stable Fe replacement site on the (110) surface of γ-alumina has been found to be represented by the tri-coordinated Fe_I position with the quartet spin state. The replacement of Al by Fe atom on Al site leads to charge redistributions of the neighboring O atoms. However, sublayer charge distribution is less affected.

The significant contribution of p orbital of the O in the surface phase to the LUMO has been founded for the tri-coordinated Fe_I substitution on (110) surface. The corresponding oxygen atoms (O_A and O_A1) have been activated due to the existence of Fe_I in their neighborhood. The loosened neighboring Al_{III}—O_A bonds match this activation. This activation of O suggests an existence of important source of the reactive O during the Fe catalytic oxidation of CO processes.

Introduction

Applications of the single metal atoms have been extensively advanced in catalytic processes.[1-20] Supported single-site metal atoms have been applied in catalyzing oxidation of CO,[1, 6-16] in reforming reactions,[17, 18] and in generating biofuels and biomass-derived chemicals by conversion of oxygen-rich biomass through hydro-deoxygenation process.[19] A catalyst with Fe supported on SiO_2 has been demonstrated to have extraordinary activity and selectivity for direct nonoxidative conversion of methane.[20] Single Pt and Au atoms supported on ZnO demonstrated tremendous activity for reformation of methanol to H_2 and CO_2.[17] Heterogeneous catalysts containing single-site metal species have also been reported serving as effective catalysts for various reactions, such as single site Pd species framed in mesoporous organosilica for oxidative Heck reaction[21] and single site Ni-modified Zn-MOF with high selectivity for dimerization of ethylene.[22]

The catalytic characteristics of these single metal atoms on various supports have been reported to be very sensitive to the electronic and geometric surroundings of the support.[23] The electronic structures of single-atom sites can be affected by the interacting atoms encircled, which might result in different catalytic behaviors as compared to single-atom sites on nonmetallic support.[23-32] The variation of electronic

and geometric surroundings of supports can provide new perceptions for activity and selectivity as well as for catalyzing effects.

It has been reported that alumina is a promising support for single-site atoms catalysts.[1-5, 15, 16] Al_2O_3 can serve as effective supports to stabilize single atoms and even to improve the catalytic activities of these single site atoms in the catalytic processes.[15, 16, 33-36] One of the important phases of this oxide, determined and widely used by experimental investigations is the so-called gamma-alumina (γ-Al_2O_3).[37, 38] Typically, γ-Al_2O_3 can be described as a defective spinel structure in which the Al vacancy sites are distributed within the lattice.[38-41]

Experimental and theoretical modeling on low-index surface indicates that the presence of penta-coordinated Al sites[34, 35, 41, 42] and tri-coordinated Al centers is particularly important in the formation of active centers of catalysts.[33, 39, 40, 43-49] Studies of the activation of methane on the γ-Al_2O_3 surfaces suggest that the highly reactive acid-base pairs created at the tri-coordinated Al enable low-energy pathways for the heterolytic splitting of C—H bond of methane.[43, 44] Recent studies demonstrate that a newly uncovered form of (111) surface provides support for three types of structural stable tri-coordinated single Fe sites on the γ-Al_2O_3 surface.[50, 51] Other researches reveal the equal importance of the tetra-coordinated Al sites on the (110) surface of γ-Al_2O_3 in single-site atoms catalysts.[4, 33, 39, 40] Different from the (111) surface, the most stable (110) surface of γ-Al_2O_3 provides three tetra-coordinated Al sites and one tri-coordinated Al site.

As an extension of our previous studies on the formation of the γ-Al_2O_3 supported tri-coordinated Fe single-site complexes, here we report the local coordination and the in-site electronic structures of the Fe single-atom sites on the (110) surface of γ-Al_2O_3. Such studies can provide deep-rooted understandings and new outlooks for the activities, selectivity, and possible catalytic effects of these γ-Al_2O_3 supported single-atom Fe complexes.

Method of computations.

The DFT method along with functional by Peverati and Truhlar (MN12-L)[52] has been used in present study. Different from the traditional surface studies using the plane wave basis such as in Vienna ab initio simulation package (VASP)[53, 54], here the localized basis set, namely the split valence basis set SV by Ahlrichs and coworkers[55] was applied. Previous studies demonstrated that reasonable estimations of the cell volume were achieved by the MN12-L functional (with double and triple zeta basis sets, i.e. SV and TZV).[50, 51] The relatively small differences in the predictions of the cell volume between the MN12-L/SV and MN12-L/TZV confirm the convergence in respect to the basis sets. This indicates a rational description of Al—O interactions in the γ-alumina by applied here functional approach. On the other hand, the significant overestimation of the cell volume by the PBEPEB approach suggests underestimating the Al—O bonding in the gamma alumina.[51] Therefore, the application of MN12-L functional is a good

tactic for the computational investigation of the gamma alumina systems. As a reliable compromise between the accurateness and the computational feasibility, the MN12-L/SV approach is applied in the following calculations. Periodic boundary conditions were applied for the description of the bulk phase. The total k-point numbers amount to 4×6×6 (for the supercell) for the bulk phase. For the computations of the surfaces phase, 2-dimensional periodic boundary conditions were applied. The total k-point number is 10×10 in the surface phase computations. The conventional convergence criteria (Maxi Force < 0.00045 au, RMS Force < 0.00030 au, Maxi Displacement < 0.0018 A, RMS Displacement < 0.0012 A, and the Predicted Change in Energy < 1.0×10^{-6} au.) of Gaussian Program was been applied in the optimization. During the computations of the bulk phase both atoms and the cell parameters were fully optimized. For the study of the surface the positions of all of the atoms were fully optimized while the corresponding lattice vectors were kept fixed. It is important to note that application of 2-dimensional periodic boundary condition implies infinity vacuum above the studied surface. Therefore, the artificial long-range interactions between the surfaces are excluded by this method. The Gaussian-09 package of programs [55] was applied for all computations.

The unit cell of the gamma alumina in bulk phase was constructed according to the well-documented crystallographic data by Digne et al (**Figure 1**).[39] [40] The supercell of the rectangular form of the model was constructed by superposition of two unit cells along *a* direction and was fully optimized by DFT approach under the periodical boundary conditions. The computed bulk structural parameters are

summarized in **Table 1**. One of the most reliable experimental parameters of the unit cell is the cell volume. The experimental cell volume of 46.39 $Å^3/Al_2O_3$ of gamma alumina[37] was adapted for verifying the methods and the basis sets used in the present study. The significant overestimation of the cell volume by the PBEPEB approach (by 2.57 $Å^3/Al_2O_3$) suggests that the PBEPBE functional underestimates the Al—O bonding in the gamma alumina. Reasonable estimations of the cell volume by the MN12-L functional (with double zeta basis sets, overestimated by 0.56 $Å^3/Al_2O_3$) indicate a rational description of Al—O interactions in the gamma alumina. The relatively small differences in the predictions of the cell volume between the MN12L/SV and MN12-L/TZV indicate it convergences with respect to the basis sets. Therefore, the MN12-L functionsl is a reasonable approach for the computational investigation of the gamma alumina systems. As a good compromise between the accuracy and the computational feasibility, the MN12-L/SV approach is applied in the following calculations.

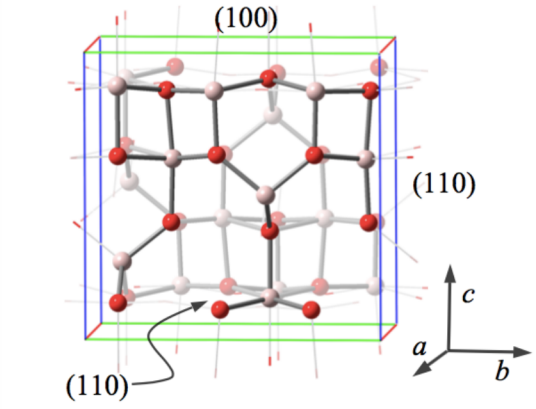

Figure 1. Unit cell of the γ-alumina in bulk. Build based on Ref. 39. Color legends: red for O and light pink for Al.

Table 1. The structural parameters of the surpercell in rectangular form,

optimized by MN12-L/SV approach. Unit of cell volume is ($Å^3/Al_2O_3$). Space group P21/m.

Method	a(Å)	b(Å)	c(Å)	α(°)	β(°)	γ(°)	Cell volume
MN12-L/SV	11.104	8.357	8.091	90.01	91.22	90.13	46.94
MN12-L/SV[a]	5.554	8.366	8.092	90.05	91.21	90.15	46.94
MN12-L/TZV[a]	5.526	8.317	8.055	90.05	91.17	90.11	46.27
PBEPBE/TZV[a]	5.625	8.490	8.205	89.99	91.01	89.99	48.96
PW91[b]	5.587	8.413	8.068	90.00	90.59	90.00	47.40
Expl.[c]							46.39

[a] Based on unit cell. Refs. 50, 51

[b] VASP calculations, using the plane wave basis. Ref. 39

[c] Experimental results. Ref. 37

Results and discussions

1. (110) surface

1.1. Selection of (110) surface

The model by Digne et al provides a good compromise between the structure reliability and the sizes compatible with quantum chemical calculations.[39] The rectangular cell unit provides a direct way to select the (110) surface by cutting along the ***a*** direction of the cell unit (or **bc** plane, see **Figure 1**). A supercell model consisting of eight atomic planes (two unit cells, 2x1x1, 80 atoms and 800 electrons) in the (110) crystallographic direction was commonly used in the surface computational studies.[4, 33] However, there are several different ways to choose (110) type of surface based on the orthogonal cell model. For each selection the surface contains one four-coordinated Al, three six-coordinated Al's, and six connecting O's. In present study, three different (110) surfaces have been selected for the stability evaluation. **Figure 2** illustrates the selections of the

surfaces, in which the (110) surface reported by the previous studies[33] is included.

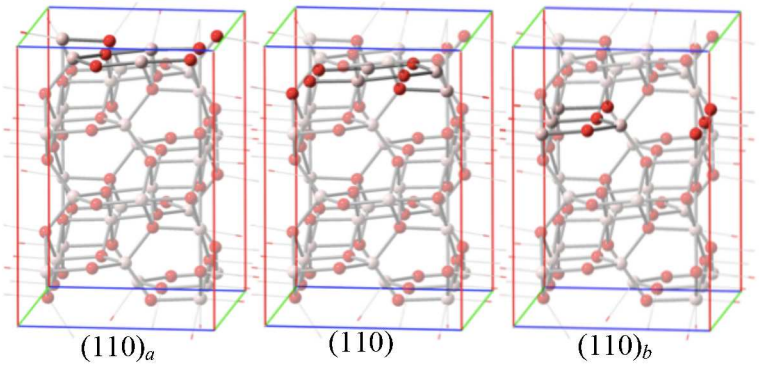

Figure 2. Selections (color intensified) and labels of the (110) surface. Left: $(110)_a$; Middle: (110); Right: $(110)_b$. The middle one is the same as the one used in the previously reported studies.[33,39,40] Color legends: red for O and light pink for Al.

The surface energies of the non-optimized surfaces are computed to be 4.259 J/m^2 for $(110)_a$, 3.739 J/m^2 for (110), and 4.791 J/m^2 for $(110)_b$ at the MN12-L/SV level of theory, respectively. Geometry relaxations lead to the reducing of the surface energy by around 1 J/m^2 (see **Table 2**). The corresponding surface energies of the optimized surfaces are calculated to be 3.233 J/m^2 for $(110)_a$, 2.961 J/m^2 for (110), and 3.592 J/m^2 for $(110)_b$, respectively. The previously reported (110) surface[33, 39, 40] has the lowest surface energy and therefore the discussions below only focus on this selected surface. It is important to note that the surface for each selection contains one four-coordinated Al, three six-coordinated Al's, and six connecting O's in the bulk. Moreover, the surface densities of Al—O bond broken are the same, 20.7 bonds/nm^2, for these three selections. The notable differences in the surface

energies indicate that the surface stability is strongly correlated to the local structures of surface. Based on the surface energy, (110) and $(111)_n$ surfaces have the similar stability, and therefore, both have the same probability of occurrence.

Table 2. The surface energies of the selected (110) and $(111)_n$ surfaces (in J/m^2)[a]

	(110)	$(110)_a$	$(110)_b$	$(111)_n$[b]
$E_{Non\text{-}opt}$	3.739	4.259	4.791	3.903
E_{opt}	2.961	3.233	3.592	2.993
ΔE	0.778	1.026	1.199	0.910

[a] $E_{Non\text{-}opt:}$ geometry non-relaxed; E_{opt}: geometry fully relaxed; $\Delta E = E_{Non\text{-}opt} - E_{opt}$. Calculated at the MN12-L/SV level of theory.
[b] $(111)_n$ surface energy see Ref. 51.

1.2. Local structure.

The geometry optimized (110) surface of supercell is depicted in **Figure 3**. The top view of the optimized surface layer of (110) is also shown in the figure in which only two layers of atoms underneath the surface have been displayed for clarity. The optimized (110) surface consists of one three-coordinated Al_I and three four-coordinated Al (one II type and two III type). The three-coordinated Al_I on the surface is derived from the four-coordinated Al in bulk phase. The dihedral D_{1AA1I} angle on the surface is computed to be 14.42°, by 18.24° smaller than that in the bulk phase. The corresponding Al_I—O bond lengths are reduced to 1.7810 Å for Al_I—O1 and 1.7180 Å for both Al_I—O_A on the (110) surface, about 0.02 Å to 0.06 Å decreases as compared to those in bulk. More pronounced Al—O bond

lengths decreases are found for Al_{III}—O_A (1.735 Å) and Al_{III}—O_C (1.842 Å). They are by about 0.10 Å and 0.12 Å shorter as compared to those in the bulk. The most profound Al—O bond tighten is found for Al_{II}—O_B (1.717 Å), about 0.17 Å shorter than the corresponding bonds (1.889 Å) in the bulk. The overall results of these Al—O bonding augmentations are that O_A and O_A1 are noticeable out of the surface (ca. 0.6 Å above the slab plane, defined by Al_{III} long with the cell plane), as can be seen from **Figure 3**. For comparison, O_A (and O_A1) is about 0.2 Å away from the slab plane in the bulk phase.

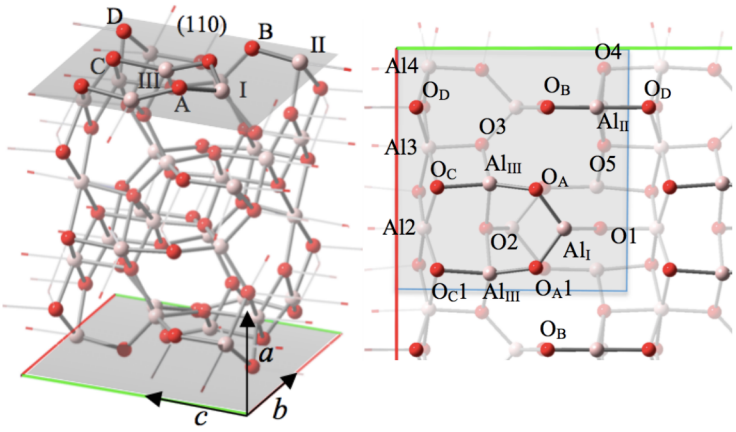

Figure 3. The optimized (110) surface supercell (left). Right panel is the top view, in which only two layers of atoms underneath the surface have been displayed for clarity. Color legends: Red for O; White for Al. The grey shade represents the (110) surface plane of the supercell.

Table 3. Geometric parameters of the local structure of the surface (110), optimized by MN12-L functional with basis sets SV.[a]

	Surface	Bulk	Δ
Al_I—O1	1.781	1.803	0.022
Al_I—O_A	1.718	1.778	0.060
Al_I—O_A1	1.718	1.778	0.060
Al_{II}—O4	1.895	1.971	0.076
Al_{II}—O5	1.895	1.971	0.076
Al_{II}—O_B	1.717	1.889	0.172
Al_{II}—O_D	1.815	1.902	0.087

Al_{III}—O2	1.885	1.942	0.057
Al_{III}—O3	1.756	1.858	0.102
Al_{III}—O_A	1.735	1.838	0.103
Al_{III}—O_C	1.842	1.958	0.116
Al2—O_C	1.814	1.841	0.027
Al3—O_C	1.888	1.969	0.081
Al3—O_D	1.882	1.979	0.097
Al4—O_D	1.881	1.979	0.098

[a] Al—O atomic distance in Å， labels see **Figure 3**.

1.4. Electron density distribution, DOS, and MO analysis

As revealed by the analysis of the density of state (DOS) in **Figure 4**, the energy gap is dominated by the surface phase and is estimated to be 3.90 eV. Compared to those in bulk phase, the electron density of Al in the surface phase is larger, increasing from 0.04 au (Al_I) to 0.35 au (Al_{II}). Meanwhile, the electron density of the oxygen on the surface (110) decreases by 0.05 au (O_C) to 0.23 au (O_D) as compared to those in bulk. The electron density distribution on the surface shows that Al_I is only slightly less positive than Al_{II} and Al_{III} and therefore, these Al atoms are expected to have similar tendency to accept or donate electrons. The analysis of the projected density of state (PDOS, **Figure 4**) clearly indicates that the occupied states near the band gap are dominated by the orbitals of O atoms in the surface layer, while the unoccupied states closest to the band gap are mainly determined by the orbitals of the corresponding Al atoms (Al_I and Al_{III}) on the surface. Specifically, the highest occupied molecular orbital (HOMO) is the combination of the p type orbitals (in-planar px or py) of oxygen atoms ($2O_A$ and O_B, see Figure 3, right panel). The HOMO-1 and HOMO-2 show the feature of the out-of-planar pz orbital of O_B and O_D (see Figure 3, right panel), respectively.

Thus, O_B and O_D are expected to be active in electron donating processes on (110) surface. On the other hand, the lowest unoccupied MO (LUMO) is found to be the sp^3 type MO of Al_I (**Figure 5**). Thus, Al_I should be active in accepting electron-rich ligands.

Table 4. Mulliken charge of the local structure of the surface (110).[a]

	Surface	Bulk	Δ
Al_I	1.77	1.81	-0.04
Al_{II}	1.83	2.17	-0.34
Al_{III}	1.86	2.16	-0.30
O1	-1.23	-1.30	0.07
O2	-1.32	-1.30	-0.02
O3	-1.32	-1.28	-0.04
O4	-1.26	-1.24	-0.02
O5	-1.26	-1.24	-0.02
O_A	-1.08	-1.28	0.20
O_B	-1.13	-1.31	0.18
O_C	-1.18	-1.22	0.04
O_D	-1.07	-1.30	0.23

[a] Analysis based on the density calculated by MN12-L functional with basis set SV. Labels see **Figure 3**. Δ = Density(Surface) – Density(Bulk).

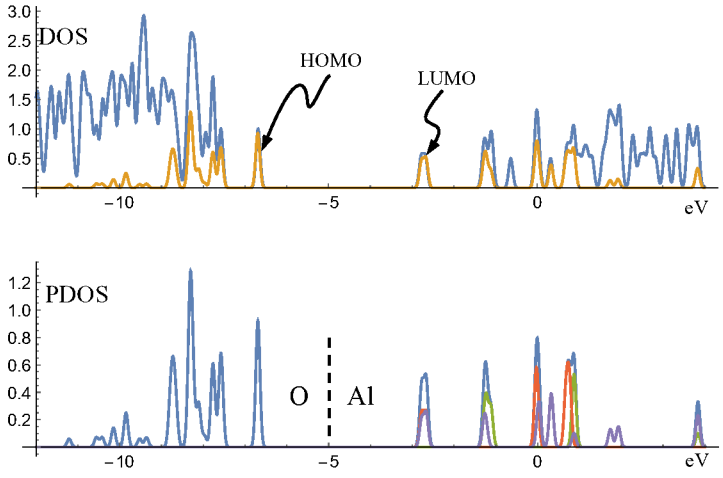

Figure 4. DOS of the (110) surface phase of γ-Al_2O_3. Upper panel is the DOS of the suppercell model (blue line) along with the contributions of the surface layer (orange line). The surface layer consists of four Al's and six O's (Al_I, Al_{II}, $2Al_{III}$, $2O_A$, O_B, $2O_C$, and O_D; see **Figure 3**). Bottom panel is the PDOS of the surface layer, in which

the part below -5 eV is the contribution from O atoms; purple line is from Al_I, green line is from Al_{II}, red line is from Al_{III}, and blue line above -5 eV is the sum of the contributions from these surface Al atoms.

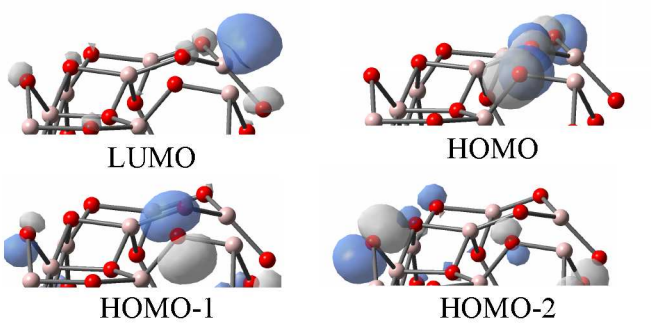

Figure 5. The frontier molecular orbitals of the surface (110). HOMO shows the combination of the p type orbitals (lying along the surface plain) of oxygen atoms.

2. Fe single sites on (110) surface of γ-Al_2O_3.

Three different types of Al sites exposed on the (110) surface (Al_I, Al_{II}, and two equivalent Al_{III}, see **Figure 3**) could be substituted by Fe atom We calculated all single atom potential substitutions. All the states with the possible spin multiplicity of Fe (doublet, quartet, and sextet) were examined. The spin quartet has been found to be the ground state for the replacements of Fe on Al_I and Al_{II} sites on (110) surface of γ-Al_2O_3. Fe replacement on the Al_{III} site results in the doublet as the ground state. In general, the replacement of Al by Fe on the surface sites of (110) surface of γ-Al_2O_3 results in formation of stable Fe-γ-Al_2O_3 systems. The energy released from the most stable substitution

Fe^{3+}(sextet) + [(110) surface of γ-Al_2O_3]

→ Al^{3+} + [Fe_I (quatet) on (110) surface of γ-Al_2O_3]

has been calculated to be 30.05 kcal/mol.

The most stable replacement site has been found to be the tri-coordinated Al_I. In terms of energy, the corresponding Fe_{II} site is about 7.62 kcal/mol less stable than that of the tri-coordinated Fe_I site. At the ground state two equivalent Fe_{III} sites are found to be 10.76 kcal/mol above the Fe_I site. In all of these sites, the high spin states (sextet) have relative high energies for Fe substituted (110) surface (see **Table 5**).

Table 5. Relative energy of the Fe substituted surface (110) of gamma alumina, optimized by MN12-L functional with basis sets SV.[a]

site	doublet	quartet	sextet
Fe_I	4.981	0.000	17.576
Fe_{II}	9.326	7.625	24.307
Fe_{III}	10.763	17.779	30.616

[a] Site labels see **Figure 3**. Relative energy in kcal/mol.

2.1. Substitution of Fe on Al_I site.

The ground state of the tri-coordinated Fe_I is quartet, which resembles II site replacement on the $(111)_n$ surface of γ-alumina.[51] The low laying excited state doublet sits 4.98 kcal/mole above the ground state. Along with the quartet, the existence of the doublet should be important on the Fe_I substituted (110) surface. However, even the significance of the sextet state should not be ignored and, as compared to the ground state, this state is 17.58 kcal/mol higher in energy.

2.1.1. Local structure of Fe_I site.

Figure 6 illustrates the optimized structure of the Fe_I substituted (110) surface of

the supercell. Replacement of Al_I by Fe on (110) surface leads to elongations of metal—O distances, especially for the sub layer O1, as compared to the pure γ-Al_2O_3 (**Table 6**). The substitution by Fe leads to the increase of the Fe_I—O1 distances by about 0.11 Å for the ground state (quartet) and 0.09 Å for the doublet, as compared to the corresponding Al_I—O1 distance of the un-substituted (110) surface. On the other hand, the surface Fe_I—O_A elongations are less obvious (less than 0.01 Å) for both quartet and doublet states. However, these atomic distance elongations are more pronounced in the corresponding sextet, as compared to the ground state and the first excited state. In the sextet state, the elongation of Fe_I—O_1 and Fe_I—O_A atomic distances amounts to 0.13 Å and 0.06 Å, respectively, as compared to the corresponding Al_I—O distances. These large increase of Fe_I—O bond lengths in the sextet implies the weakened of bonding between Fe_I and the surface of alumina in the excited state. It is important to note that the existence of Fe_I also increases the Al_{III}—O_A distances by 0.04 Å, approximately, in the ground state (0.03 Å for the doublet and 0.02 Å for the sextet, respectively). The Al_{III}—O_A bonding seems be loosened by the replacement of Fe at the Al_I site on (110) surface.

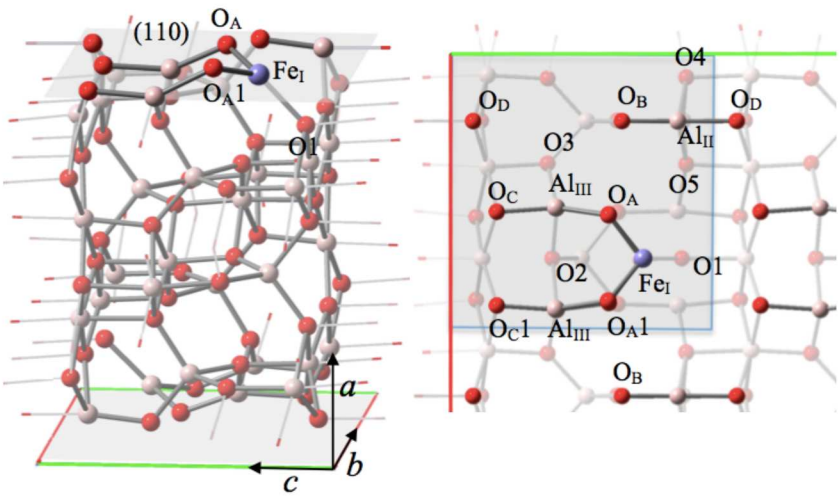

Figure 6. The structure of the fully optimized Fe_I substituted (110) surface of the supercell in ground state (quartet). Right panel is the top view. Color legends: red for O, light pink for Al, and blue gray for Fe.

Table 6. Geometries of the local structure of the Fe_I substituted surface (110) of γ-alumina, optimized by MN12-L functional with basis sets SV.[a]

	Non-substituted	Fe-substituted		
	singlet	doublet	quartet	sextet
$R_{I\text{-}1}$	1.781	1.861	1.894	1.907
$R_{I\text{-}A}$	1.718	1.722	1.725	1.783
$R_{I\text{-}A1}$	1.718	1.722	1.725	1.783
$R_{III\text{-}A}$	1.735	1.768	1.772	1.753
D_{1AA1I}	14.42	24.87	13.91	20.02

[a] $R_{I\text{-}i}$: Fe_I—O_i atomic distance for substituted surfaces (Al_I—O_i atomic distance for non-substituted surface) in Å; $R_{III\text{-}A}$: Al_{III}—O_A atomic distance in Å; D_{ijkI}: dihedral angle in (°), labels see **Figure 6**.

The dihedral angle of the Fe_I site (D_{1AA1I}) in the ground state is basically the same as compared to that of the Al_I site (13.9° vs. 14.4°). However, the increases of the corresponding dihedral angle are notable in the high spin states. The D_{1AA1I} value amounts to 24.9° for doublet and 20.0° for sextet.

2.1.2. Electron density distribution, DOS, and MO analysis of Fe_I site.

Table 7. Mulliken charge and spin density of the local structure of the surface (110).[a]

	Quartet		Doublet		Sextet	
	Charge	Spin	Charge	Spin	Charge	Spin
Fe_I	1.46	2.73	1.46	1.08	1.65	4.00
	(1.77)	(0.00)				
O1	-1.20	0.07	-1.15	-0.03	-1.19	0.11
	(-1.23)	(0.00)				
O_A	-0.90	0.07	-0.92	-0.01	-0.95	0.42
	(-1.08)	(0.00)				
O_A1	-0.90	0.07	-0.92	-0.01	-0.95	0.42
	(-1.08)	(0.00)				

[a] Analysis based on the density by MN12-L functional with basis set SV. Labels see **Figure 6**. The numbers in the parentheses are for Al_I in the non-substituted system.

The Mulliken charge analysis indicates that the substitution by Fe on Al_I site leads to charge redistributions of the surrounding O atoms. As shown in **Table 7**, the charge on the Fe_I atom is 1.46 au in the ground state. In comparison with Al_I atom, Fe_I is less charged, about 0.31 au on the (110) surface. Accordingly, the O atoms around the Fe_I are less charged as compared to the non-substituted system. On the surface layer, the charge densities on the O_A and O_A1 atoms are calculated to be -0.897 au, while those charges amount to -1.182 au for both atomic sites in the non-substituted surface. Small charge variation is detected in the sublayer, the charge on O1 amounts to -1.196 au, about 0.04 au less negative than that in the non-substituted system. Sub layer charge distribution seems to be less affected by the Fe_I substitution on (110) surface as compared to the surface layer. Similar charge variation trend can also be identified for the doublet and sextet, in which the sub layer O1 shows less than 0.1 au in charge alteration (0.04 to 0.09 au)

while on layer O_A and O_A1 one predicts charge difference of more than 0.1 au (0.14 to 0.17 au) as compared to the non-substituted alumina system.

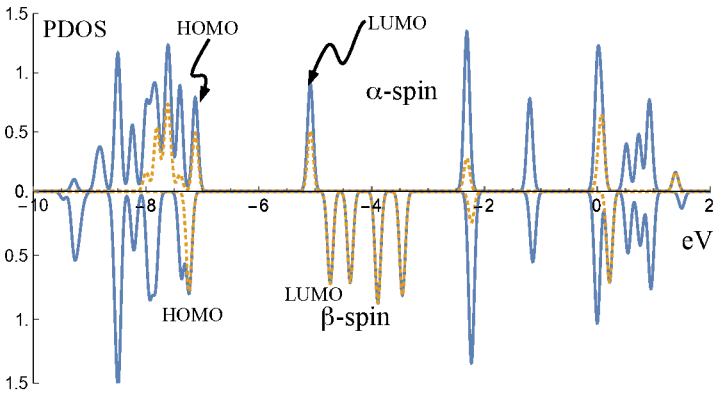

Figure 7. PDOS of the Fe_I substituted (110) surface phase of γ-Al_2O_3 in quartet state. The surface layer consists of one Fe, three Al atoms, and six O atoms (Fe_I, Al_{II}, $2Al_{III}$, $2O_A$, O_B, $2O_C$, and O_D; see **Figure 6**). Blue line is from the surface layer and the dotted orange line is the contribution from Fe_I. The contribution of oxygen atoms is included in the PDOS of the surface layer (Blue line, in the area of energy lower than HOMO) and the contribution of Al atoms is included in the PDOS of the surface layer (Blue line, in the area of energy larger than LUMO).

The analysis of the projected density of state (PDOS, **Figure 7**) reveals that the occupied states near the band gap are dominated by the orbitals of Fe and O atoms in the surface layer, while the unoccupied states closest to the band gap are mainly determined by the orbitals of the corresponding Fe atom. The HOMO-LUMO gap (band gap) is predicted to be 2.04 eV (α-spin) and 2.50 eV (β-spin) for the ground state of the Fe_I substituted (110) surface system. This band

gap is only half of that of un-substituted (110) surface of γ-Al_2O_3. The MO analysis of this system reveals that the d-type orbitals of the tri-coordinated Fe dominate the frontier MO's (**Figure 8**).

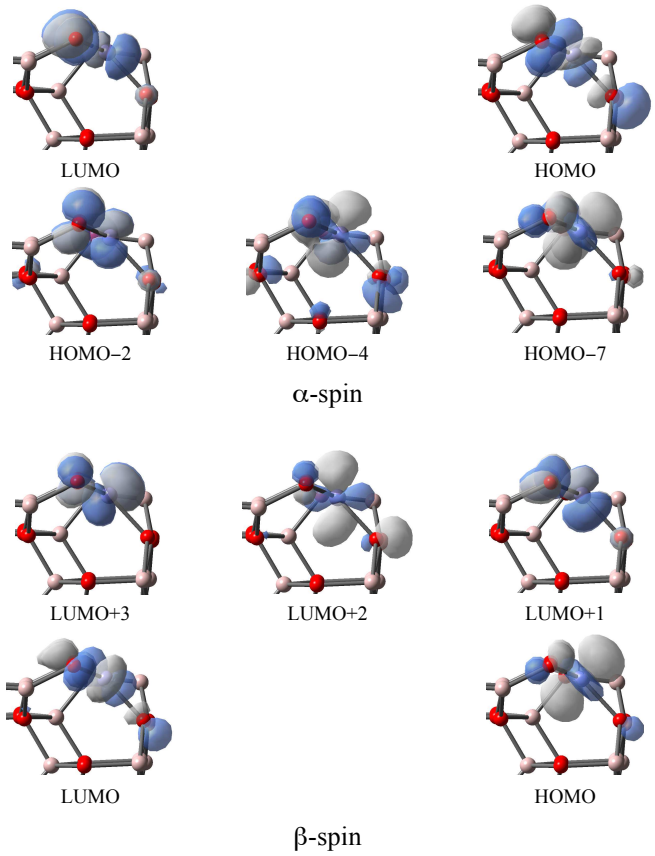

Figure 8. The frontier MO's associated with the band gap for the ground state (quartet) of the Fe_I substituted (110) surface of γ-alumina. They are all related to the d orbitals of Fe_I.

The d-type orbitals of Fe_I mainly appear in HOMO, HOMO-2, HOMO-4, and HOMO-7 for the α-spin orbitals and in HOMO for the β-spin orbitals. For the un-occupied frontier MO's, a d-type orbital of Fe_I mixed with the p-type orbitals of O (O_A and O_A1) constructs the LUMO for α-spin states. On the other hand, d-orbitals of Fe dominate the low-laying unoccupied frontier MO's, from LUMO

to LUMO+3. Therefore, the band gap in the Fe_I substituted (110) surface of γ-alumina is mainly determined by the d orbital splitting patterns of the inserted Fe atom. The PDOS analysis of the (110) surface of the pure γ-alumina revealed that the MO's of the surface O atom do not participate in unoccupied band (see **Figure 5**). The significant contribution of p orbital of O_A and O_A1 to the LUMO of the Fe_I-γ-Al_2O_3 surface indicates that these two oxygen atoms have been activated due to the replacement by Fe on the Al_I site. The loosened Al_{III}—O_A bonds (0.04 elongation in bond length) match this activation. This activation of O might be important source of the reactive O during the Fe catalytic oxidation of CO to CO_2 processes.

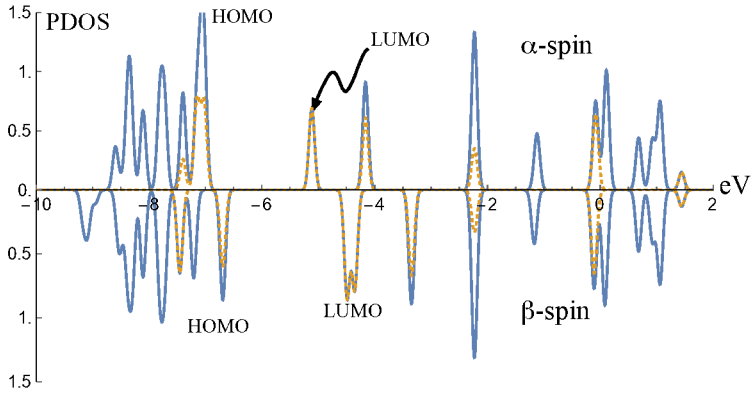

Figure 9. PDOS of the Fe_I substituted (110) surface phase of γ-Al_2O_3 in doublet. The surface layer consists of one Fe, three Al atoms, and six O atoms (Fe_I, Al_{II}, $2Al_{III}$, $2O_A$, O_B, $2O_C$, and O_D; see **Figure 6**). Blue line is from the surface layer and the dotted orange line is the contribution from Fe_I. The contribution of oxygen atoms is included in the PDOS of the surface layer (Blue line, in the area of energy lower than HOMO) and the contribution of Al atoms is included in the PDOS of the surface layer (Blue line, in the area of energy larger than LUMO).

The band gap of the doublet state is computed to be 1.91 eV for α-spin part and

2.20 eV for β-spin part, close to those of the ground state. Similar to the case of the quartet, the band gap is largely determined by the d orbital splitting patterns of the Fe_I on (110) surface of γ-alumina. Although the p-type orbitals from O_A and O_A1 do not contribute to the LUMO, their non-negligible contributions to the LUMO+1 (see **Figure S1** in Supporting Information, SI) suggest that these two O's are also activated in the presence of Fe_I on the surface in the doublet state, a reasonable concord of the elongations of the Al_{III}—O_A bonds in the low-laying excited state of the Fe_I-γ-Al_2O_3 (110) surface.

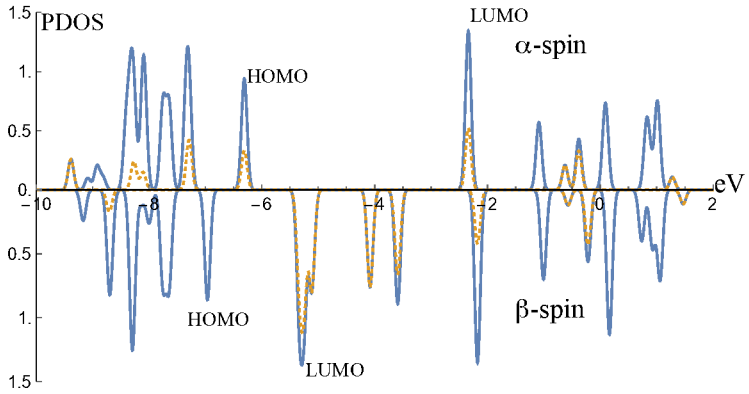

Figure 10. PDOS of the Fe_I substituted (110) surface phase of γ-Al_2O_3 in sextet. The surface layer consists of one Fe, three Al atoms, and six O atoms (Fe_I, Al_{II}, $2Al_{III}$, $2O_A$, O_B, $2O_C$, and O_D; see **Figure 6**). Blue line is from the surface layer and the dotted orange line is the contribution from Fe_I. The contribution of oxygen atoms is included in the PDOS of the surface layer (Blue line, in the area of energy lower than HOMO) and the contribution of Al atoms is included in the PDOS of the surface layer (Blue line, in the area of energy larger than LUMO).

PDOS analysis reveals that the band gap of the sextet state is 3.92 eV for α-spin, close to that of the pure (110) γ-Al_2O_3 surface (3.90 eV). MO analysis indicates that the contribution of d orbital of Fe_I to the occupied frontier MO's (HOMO and

HOMO-1, see **Figure S2 in** SI) and the involvement of s orbital of Fe_I in the LUMO barely alters the band gap of the α-spin component. On the other hand, while the occupied band originates basically from the O atoms of the surface, the vacant band of the β-spin component is dominated by the unoccupied d orbitals of Fe_I, resulting in a small band gap of 1.63 eV for β-spin. Unlike the quartet and doublet, the band gap in sextet state does not depend on the d orbital splitting of the Fe_I on (110) surface of γ-Al_2O_3. Activation of O_A and O_A1 can be characterized by the mixing of p orbitals of O_A and O_A1 with d orbitals of Fe_I, recognizable in LUMO, LUMO+1 and LUMO+4 of the β-spin components. It is the interaction between the p orbitals of O_A (also O_A1) and the d orbital of Fe_I that leads to significant spin density transfer from Fe_I to O_A (also O_A1) as shown in the results of Mulliken population analysis (**Table 7**).

2.2. Substitution of Fe on Al_{II} site.

The ground state of the tetra-coordinated Fe_{II} is quartet that is 7.63 kcal/mol less stable than that characterizing the tri-coordinated Fe_I. The low laying excited state doublet is 1.70 kcal/mole above the corresponding ground state. Both of the doublet and quartet should be important for the tetra-coordinated Fe_{II} on the (110) surface of γ-Al_2O_3. The involvement of the sextet state on this surface should also not be ignored. The energy of the sextet is by 13.68 kcal/mol higher than that of the ground state.

2.2.1. Local structure of Fe_{II} site.

Table 8. Geometries of the local structure of the Fe_{II} substituted surface (110) of γ-alumina, optimized by MN12-L functional with basis sets SV.[a]

	Non-substituted	Fe-substituted		
	singlet	doublet	quartet	sextet
$R_{II\text{-}4}$	1.895	1.910	2.028	2.058
$R_{II\text{-}5}$	1.895	1.910	2.017	2.058
$R_{II\text{-}B}$	1.718	1.736	1.706	1.753
$R_{II\text{-}D}$	1.815	1.884	1.818	1.873
$R_{Al5\text{-}B}$	1.742	1.765	1.775	1.770
D_{1ID4B}	3.28	1.07	-1.25	-2.54

[a] $R_{II\text{-}i}$: Fe_{II}—O_i atomic distance for substituted surfaces (Al_{II}—O_i atomic distance for non-substituted surface) in Å; $R_{Al5\text{-}B}$: Al5—O_B atomic distance in Å; D: dihedral angle in (°), labels see **Figure 11**.

The optimized structure of the Fe_{II} substituted (110) surface of the supercell is presented in **Figure 11**. Substitution by Fe_{II} on (110) surface leads to elongations of metal—O distances, especially for the sub layer O4 and O5, as compared to the pure γ-Al_2O_3 (**Table 8**). The substitution by Fe results in the Fe_{II}—O4 (and O5) distances of 2.028 Å (2.017 Å) for the ground state (quartet), about 0.13 Å longer than the corresponding Al_{II}—O4 bond length of the pure alumina (110) surface. In the doublet state, the Fe_{II}—O4 is computed to be 1.910 Å, about 0.11 Å shorter than that in the ground state. The interaction between Fe_{II} and the sub layer is stronger in the doublet state as compared with that in the quartet. In the ground state, the in-surface Fe_{II}—O bond lengths are short, 1.706 Å for Fe_{II}—O_B and 1.818 Å for Fe_{II}—O_D, respectively. Based on the bond length, the bonding between O_B and Fe_{II} is stronger than that between O_D and Fe_{II}. Similar bonding preference of Fe_{II} is also noted in the doublet and the sextet states (see **Table 8**). The Fe_{II}—O_B bond length is 1.736 Å and the Fe_{II}—O_D bond length is 1.884 Å in

the doublet, and they are 1.753 Å and 1.873 Å, respectively, in the corresponding sextet state. The inter layer Al15—O_B increases to 1.765 ~ 1.775 Å in the Fe_{II} substituted (110) surface of γ-alumina, while it is 1.742 Å in the non-substituted alumina. The inter layer Al5—O_B bonding is weakened due to the presence of Fe_{II} on the (110) surface.

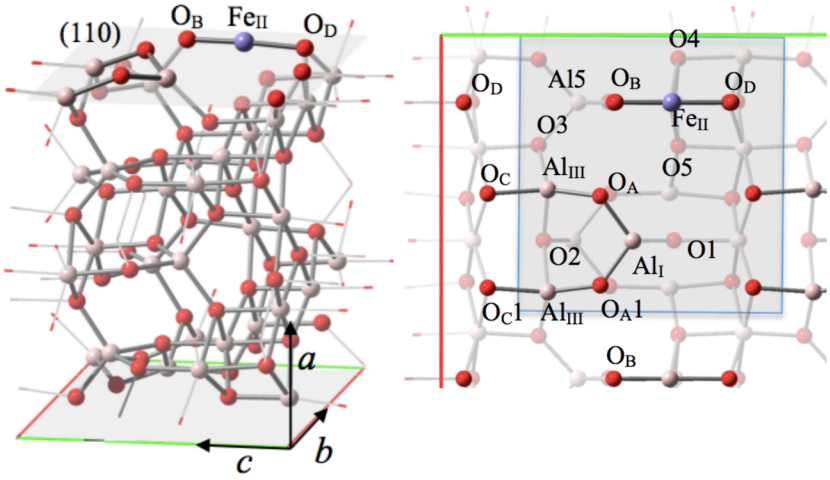

Figure 11. The structure of the fully optimized Fe_{II} substituted (110) surface of the supercell in ground state (quartet). Right panel is the top view. Color legends: red for O, light pink for Al, and blue gray for Fe.

2.2.2. Electron density distribution, DOS, and MO analysis of Fe_{II} site.

Charge redistributions of the surrounding O atoms caused by introduction of Fe_{II} on the (110) surface were revealed by Mulliken charge analysis shown in **Table 9**. The charge on the Fe_{II} atom is 1.57 au in the quartet state. The O atoms around the Fe_{II} are less charged as compared to the non-substituted system. On the surface layer, the charge densities of the Fe_{II} tightly bonded to O_B is calculated to be -0.887 au, about 0.19 au less than that on the non-substituted surface. The

charge density of the loosely bonded O_D amounts to -1.014 au, approximately 0.12 au less than that in the non-substituted alumina. In the sublayer, charge variation caused by Fe_{II} is less significant. The charge on O4 (and O5) amounts to -1.178 au, about 0.08 au less negative than that in the non-substituted system. The charge alteration is in accordance with the bonding strength of Fe_{II}—O on the surface. Similar charge variation trend can be recognized for the doublet and sextet, in which the sub layer O4 (and O5) and the loosely bonded O_D are characterized by less than 0.1 au of charge alteration (roughly 0.09 au) while on layer O_B atom displays more than 0.1 au of charge difference (0.17 au), in comparison to the pure alumina.

In the low-laying excited state (doublet) the charge density on Fe_{II} is slightly more positive (about 0.01 au) as compared to that in the ground state. However, notable positive charge increase on Fe_{II} has been identified (0.10 au approximately) in the sextet state, the charge on Fe_{II} is 1.668 au in this state. Excitation moves the electron density away form the central Fe atom. Consequently, the loosely bonded O_D receives about 0.04 au of electron density from Fe_{II} in the doublet and in the sextet, respectively, due to the excitation.

Table 9. Mulliken charge and spin density of the local structure of the surface (110).[a]

	Quartet		Doublet		Sextet	
	Charge	Spin	Charge	Spin	Charge	Spin
Fe_{II}	1.57	2.68	1.58	0.92	1.67	4.13
	(1.83)	(0.00)				
O4	-1.18	0.01	-1.16	-0.02	-1.17	0.11
	(-1.26)	(0.00)				

O5	-1.18	0.01	-1.16	-0.02	-1.17	0.11
	(-1.26)	(0.00)				
O_B	-0.89	0.21	-0.90	0.11	-0.91	0.46
	(-1.07)	(0.00)				
O_D	-1.01	-0.06	-1.05	0.00	-1.05	0.19
	(-1.13)	(0.00)				

[a] Analysis based on the density by MN12-L functional with basis set SV. Labels see **Figure 11**. The numbers in the parentheses are for Al_{II} in the non-substituted system.

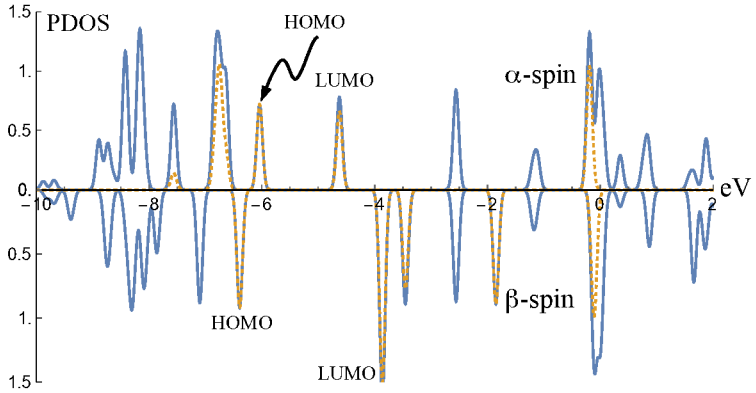

Figure 12. PDOS of the Fe_{II} substituted (110) surface phase of γ-Al_2O_3 in quartet state. The surface layer consists of one Fe, three Al atoms, and six O atoms (Fe_{II}, Al_I, $2Al_{III}$, $2O_A$, O_B, $2O_C$, and O_D; see **Figure 11**). Blue line is from the surface layer and the dotted orange line is the contribution from Fe_{II}. The contribution of oxygen atoms is included in the PDOS of the surface layer (Blue line, in the area of energy lower than HOMO) and the contribution of Al atoms is included in the PDOS of the surface layer (Blue line, in the area of energy larger than LUMO).

The analysis of the PDOS (see **Figure 12**) indicates that the band parts near the band gap are mainly dominated by the orbitals of Fe_{II}. The band gap is predicted to be 1.41 eV (α-spin) and 2.53 eV (β-spin) for the ground state of the Fe_{II} substituted (110) surface of γ-alumina. In comparison with the PDOS of the Fe_I substituted (110) surface system, the band gap of α-spin is slightly reduced (by 0.6 eV) while that of β-spin is increased by 0.03 eV in the corresponding Fe_{II} system. The MO arrangement of the tetra-coordinated Fe_{II} on the (110) surface is

expected to be different from that in the tri-coordinated Fe_I.

The MO analysis of this Fe_{II} substituted system disclosures that the frontier MO's are subjugated by the d-type orbitals of the tetra-coordinated Fe.

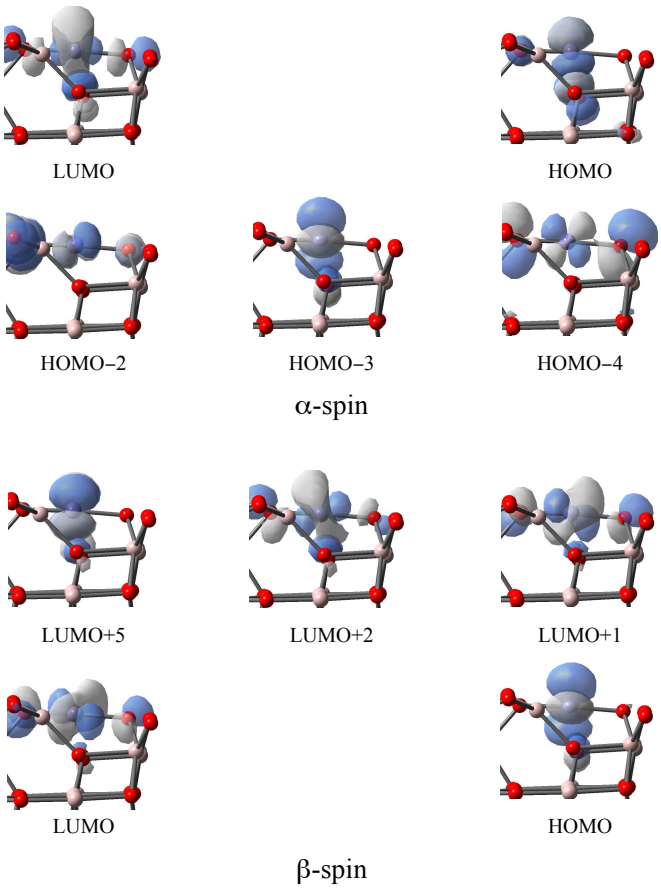

Figure 13. The frontier MO's associated to the band gap for the ground state (quartet) of the Fe_{II} substituted (110) surface of γ-alumina. They are related to the d orbitals of Fe_{II}.

The involvement of p orbitals of O_D and O_B in the LUMO suggests the partial transfer of these p orbitals from occupied band to the empty band through interactions with Fe_{II}. Consequently, this transfer leads to the increase of spin density of O_B (roughly 0.2 au, see **Table 9**), indicating the activation of this O

atom.

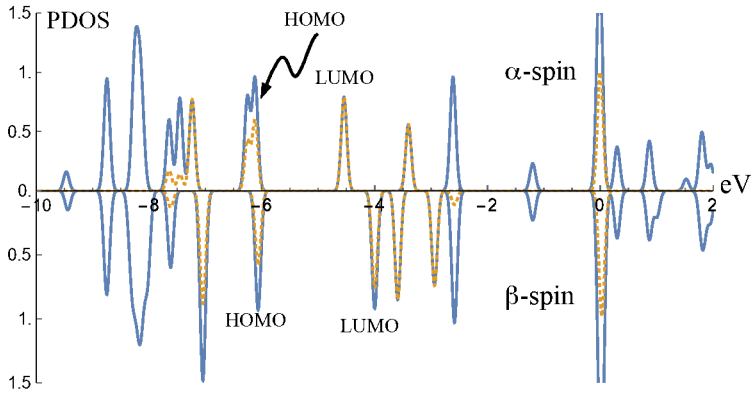

Figure 14. PDOS of the Fe_{II} substituted (110) surface phase of γ-Al_2O_3 in doublet state. The surface layer consists of one Fe, three Al atoms, and six O atoms (Fe_{II}, Al_I, $2Al_{III}$, $2O_A$, O_B, $2O_C$, and O_D; see **Figure 11**). Blue line is from the surface layer and the dotted orange line is the contribution from Fe_{II}. The contribution of oxygen atoms is included in the PDOS of the surface layer (Blue line, in the area of energy lower than HOMO) and the contribution of Al atoms is included in the PDOS of the surface layer (Blue line, in the area of energy larger than LUMO).

The projected DOS of the Fe_{II}-γ-Al_2O_3 in the low energy excited state (doublet) is depicted in **Figure 14**. The band gap is predicted to be 1.58 eV (α-spin) and 2.06 eV (β-spin) for the doublet state. Similar to the quartet, the band gap is largely controlled by the d orbital splitting patterns of the Fe_{II} on (110) surface of γ-Al_2O_3. The contributions of the p orbitals of O atoms in the surface phase to the HOMO and HOMO-1 can be detected based on the results of MO analysis (**Figure S3** in SI).

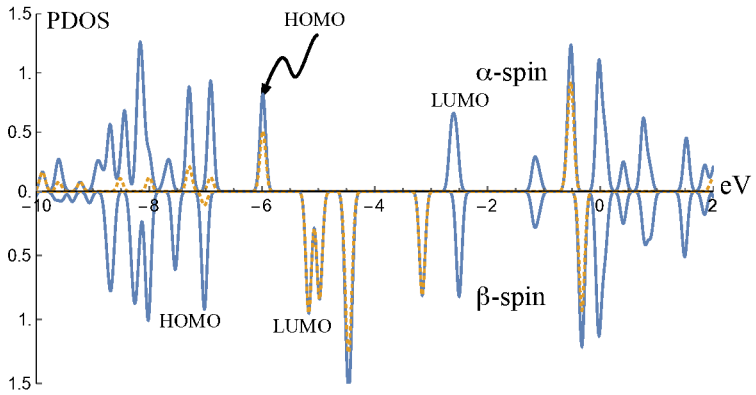

Figure 15. PDOS of the Fe_{II} substituted (110) surface phase of γ-Al_2O_3 in its sextet state. The surface layer consists of one Fe, three Al atoms, and six O atoms (Fe_{II}, Al_I, $2Al_{III}$, $2O_A$, O_B, $2O_C$, and O_D; see **Figure 11**). Blue line is from the surface layer and the dotted orange line is the contribution from Fe_{II}. The contribution of oxygen atoms is included in the PDOS of the surface layer (Blue line, in the area of energy lower than HOMO) and the contribution of Al atoms is included in the PDOS of the surface layer (Blue line, in the area of energy larger than LUMO).

PDOS and MO analysis reveals that the band gap of the sextet state is 3.35 eV for α-spin and 1.85 eV for β-spin, respectively. The band gap of the α-spin component is dominated by the occupied p orbitals of O's of the surface (with the certain contributions from the d orbital of Fe_{II}) and the unoccupied orbitals of the Al atoms of the system. On the other hand, the β-spin component is determined by the occupied p orbitals of O's and the unoccupied d orbitals of the substituted Fe_{II} on the surface (see **Figure S4** in SI). This is the case resembling the sextet state of Fe_I substituted alumina. The band gap in sextet state does not depend on the d orbital splitting pattern of the Fe on (110) surface of γ-Al_2O_3.

2.3. Substitution of Fe on Al_{III} site.

Two Al_{III} positions are equivalent due to the symmetry of the modeled γ-Al_2O_3.

The ground state of the tetra-coordinated Fe_{III} (doublet) is by 10.76 kcal/mol less stable than that of the tri-coordinated Fe_I. The low-laying excited state (quartet) is 7.02 kcal/mole above the corresponding ground state. The energy of the sextet is 19.86 kcal/mol higher than that of the ground state. The contributions of the quartet and sextet states of Fe_{III} to the properties of the surface could not be overlooked.

2.3.1. Local structure of Fe_{III} site.

Table 10. Geometries of the local structure of the Fe_{III} substituted surface (110) of γ-alumina, optimized by MN12-L functional with basis sets SV.[a]

	Non-substituted	Fe-substituted		
	singlet	doublet	quartet	sextet
R_{III-2}	1.885	1.887	2.214	2.101
R_{III-3}	1.756	1.789	1.825	1.855
R_{III-A}	1.735	1.805	1.742	1.787
R_{III-C}	1.842	1.885	1.830	1.914
R_{Al2-C}	1.814	1.802	1.839	1.819
D_{1IIA2C}	-19.69	-0.79	-5.45	-11.56

[a] R_{III-i}: Fe_{III}—O_i atomic distance for substituted surfaces (Al_{III}—O_i atomic distance for non-substituted surface) in Å; R_{Al2-C}: Al12—O_C atomic distance in Å; D: dihedral angle in (°), labels see **Figure 16**.

The optimized supercell of Fe_{III} substituted (110) surface of γ-Al_2O_3 is depicted in **Figure 16**. The substitution by Fe leads to the Fe_{III}—O2 distance of 1.887 Å and the Fe_{III}—O3 distance of 1.789 Å for the ground state (doublet). On the other

hand, the surface metal—O elongations are obvious; 0.07 Å longer for Fe_{III}—O_A and 0.04 Å longer for Fe_{III}—O_C, as compared to the corresponding Al_{III}—O distances on the (110) surface. However, the increase of bond distances is more pronounced for inter plane metal—O in the quartet state. The Fe_{III}—O2 increase is 2.214 Å and the Fe_{III}—O3 distance is 1.825 Å; for the comparison, the corresponding values are 1.887 Å and 1.789 Å in the ground state. The presence of Fe_{III} loosens the bonding between the surface layer and the bulk phase (locally) in the quartet, as further suggested by the elongated inter-layer Al—O distance (Al2—O_C, 1.839 Å). Meanwhile, the metal—O distances on the Fe_{III} substituted (110) surface are found to be close to those of the pure alumina (see **Table 10**). Fe_{III} is more tightly bonded to the surface O's as compared to the ground state. In the sextet state, the notable elongation of all Fe_{III}—O atomic distances implies that the excitation of Fe_{III} weakens the Fe–alumina bonding.

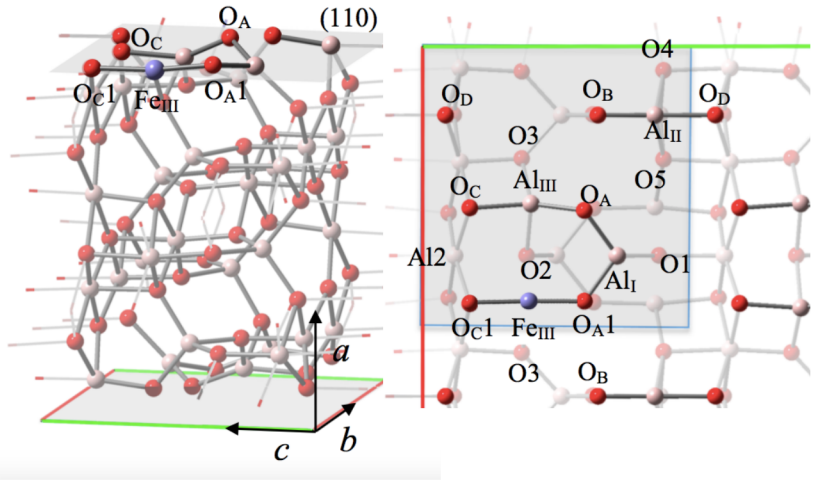

Figure 16. The structure of the fully optimized Fe_{III} substituted (110) surface of the supercell in ground state (doublet). Right panel is the top view. Color legends: red for O, light pink for Al, and blue gray for Fe.

2.3.2. Electron density distribution, DOS, and MO analysis of Fe_{III} site.

Charge redistribution of the surrounding O atoms caused by introduction of Fe_{III} on the (110) surface was analyzed by Mulliken population analysis as listed in **Table 11**. For the ground state (doublet), the charge of Fe_{III} is computed to be 1.470 au on the (110) surface while it is 2.220 au in the bulk (present study, cell optimized with one six-coordinated Al replaced by Fe in bulk phase). The charge reduction of the Fe_{III} on the surface is more pronounced than that of Al_{III} (-0.750 au vs. -0.308 au). Consequently, the O atoms around the Fe_{III} are less charged as compared to the non-substituted system. On the surface layer, the charge densities of the neighboring O atoms (O_A and O_C) of Fe_{III} are about 0.1 au less negative as compared to those of the pure alumina. Similar trends of charge alteration can also be identified for the sub layer O atoms (O2 and O3). The charge redistribution pattern of the quartet and the sextet states follows that of the ground state. In all the states studied, the notable spin density distributions on O_A (0.2 ~ 0.3) suggest the strong Fe_{III}—O_A bonding interaction, consistent with the short Fe_{III}—O_A atomic distance discussed above.

Table 11. Mulliken charge and spin density of the local structure of the surface (110).[a]

	Doublet		Quartet		Sextet	
	Charge	Spin	Charge	Spin	Charge	Spin
Fe_{III}	1.47	1.01	1.50	2.69	1.63	4.10
	(1.86)	(0.00)				
O2	-1.14	-0.03	-1.14	-0.04	-1.16	0.27
	(-1.32)	(0.00)				
O3	-1.23	-0.03	-1.27	0.05	-1.26	0.10
	(-1.32)	(0.00)				
O_A	-0.94	0.21	-0.91	0.23	-0.94	0.33

	(-1.08)	(0.00)				
O_C	-1.09	-0.01	-1.05	0.05	-1.08	0.17
	(-1.18)	(0.00)				

[a] Analysis based on the density by MN12-L functional with basis set SV. Labels see **Figure 16**. The numbers in the parentheses are for Al_{III} in the non-substituted system.

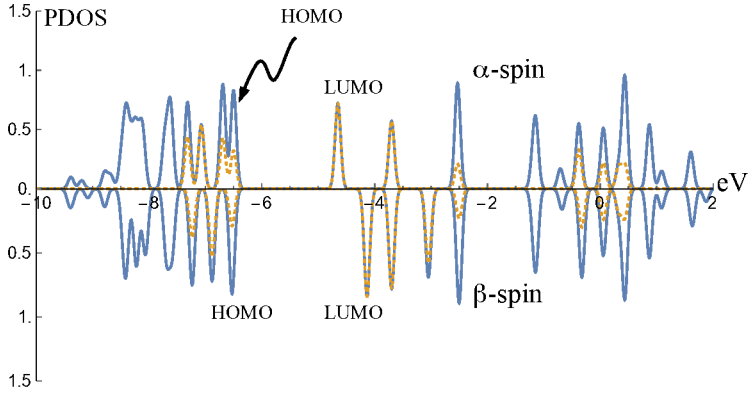

Figure 17. PDOS of the Fe_{III} substituted (110) surface phase of γ-Al_2O_3 in doublet state. The surface layer consists of one Fe, three Al atoms, and six O atoms (Fe_{III}, Al_I, Al_{II}, Al_{III}, $2O_A$, O_B, $2O_C$, and O_D; see **Figure 16**). Blue line is from the surface layer and the dotted orange line is the contribution from Fe_{III}. The contribution of oxygen atoms is included in the PDOS of the surface layer (Blue line, in the area of energy lower than HOMO) and the contribution of Al atoms is included in the PDOS of the surface layer (Blue line, in the area of energy larger than LUMO).

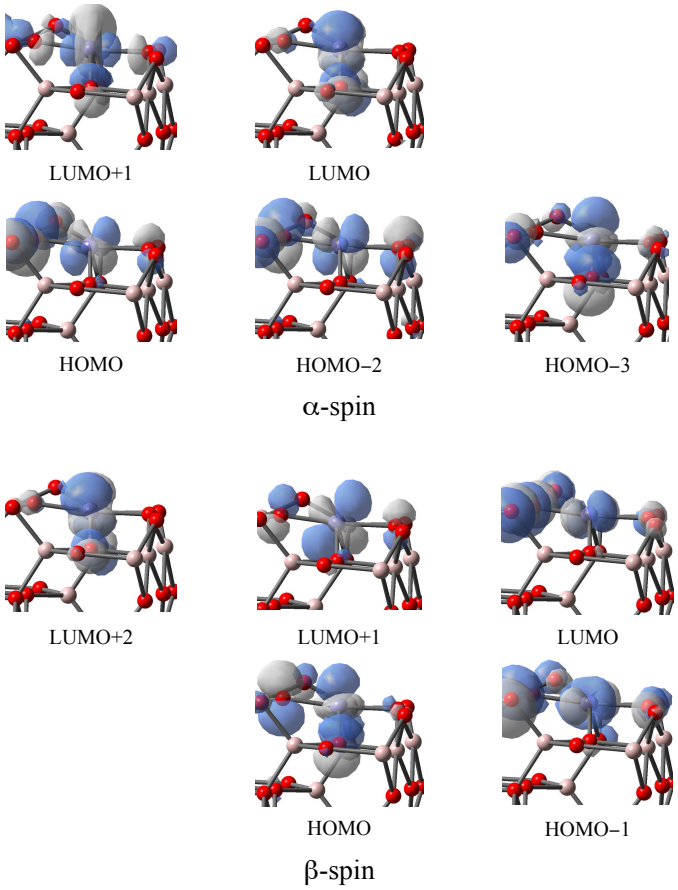

Figure 18. The frontier MO's associated to the band gap for the ground state (doublet) of the Fe_{III} substituted (110) surface of γ-alumina. They are related to the d orbitals of Fe_{III}.

The analysis of the PDOS (see **Figure 17**) reveals that the occupied band near the gap is largely the combination of the orbitals of O and the orbitals of Fe_{III}, while the empty band close to the gap is dominated by the orbitals of Fe_{III} only. The computed band gap is 1.85 eV (α-spin) and 2.39 eV (β-spin) for the Fe_{III} substituted (110) surface of γ-alumina in its doublet state. In comparison with the doublet state of the Fe_{II} substituted (110) surface system, the band gap is moderately increased (by ~ 0.3 eV) in the corresponding Fe_{III} system. Large contribution of the orbitals of the surface phase O atoms in the occupied frontier

MO accounts for this gap expansion in the Fe_{III} system.

In addition to the contributions of the d-type orbitals from the Fe_{III}, MO analysis of this Fe_{III} substituted system reveals the significant contributions of p-type orbitals of O to the occupied frontier MO's, as shown in HOMO, HOMO-2, and HOMO-3 for α-spin, and in HOMO and HOMO-1 for β-spin. Meanwhile, the main contribution to the LUMO comes from d orbital of the coordinated Fe_{III}, as shown in **Figure 18**.

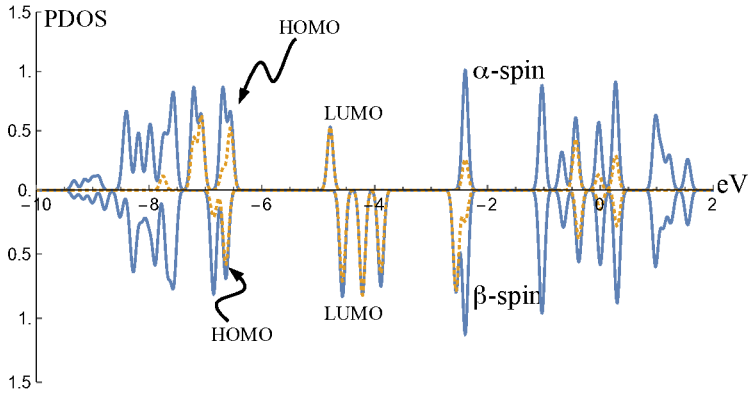

Figure 19. PDOS of the Fe_{III} substituted (110) surface phase of γ-Al_2O_3 in quartet state. The surface layer consists of one Fe, three Al atoms, and six O atoms (Fe_{III}, Al_I, Al_{II}, Al_{III}, $2O_A$, O_B, $2O_C$, and O_D; see **Figure 16**). Blue line is from the surface layer and the dotted orange line is the contribution from Fe_{III}. The contribution of oxygen atoms is included in the PDOS of the surface layer (Blue line, in the area of energy lower than HOMO) and the contribution of Al atoms is included in the PDOS of the surface layer (Blue line, in the area of energy larger than LUMO).

The PDOS of the Fe_{III} substituted (110) surface phase of γ-Al_2O_3 in quartet are depicted in **Figure 19**. The band gap is 1.77 eV for α-spin and 2.07 eV for β-spin. For α-spin component, the occupied band near the gap is determined by the combination of the orbitals of O and the orbitals of Fe_{III}, while the unoccupied band close to the gap is subjugated by the orbitals of Fe_{III} mainly. MO analysis

reveals that from HOMO to HOMO-3, the d orbitals of Fe_{III} are heavily mixed with the p orbitals from the surrounding O atoms. On the other hand, the corresponding LUMO shows chiefly the d orbital of the Fe_{III} with minor contribution from the p orbitals of the neighboring O atoms (see SI). This situation is similar to that in the doublet state with the corresponding band gap of 1.85 eV. However, the orbitals from Fe_{III} alone dominate the band close to the band gap in β-spin section. Both HOMO and LUMO reveal for the doublet the main contributions from the d orbitals of Fe_{III}. The gap is controlled by the splitting pattern of d orbitals of Fe_{III} on the (110) surface.

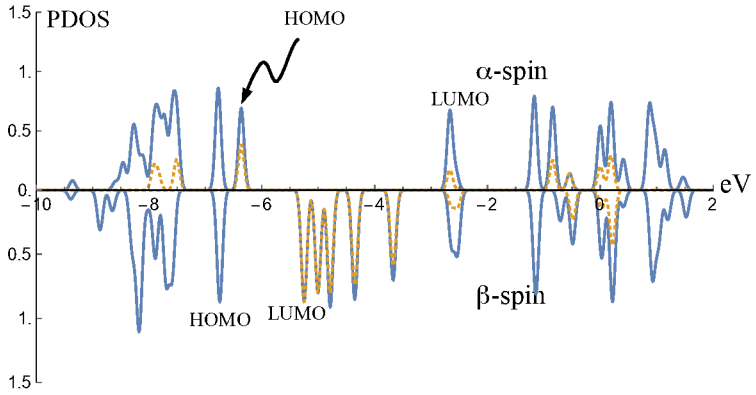

Figure 20. PDOS of the Fe_{III} substituted (110) surface phase of γ-Al_2O_3 in sextet state. The surface layer consists of one Fe, three Al atoms, and six O atoms (Fe_{III}, Al_I, Al_{II}, Al_{III}, $2O_A$, O_B, $2O_C$, and O_D; see **Figure 16**). Blue line is from the surface layer and the dotted orange line is the contribution from Fe_{III}. The contribution of oxygen atoms is included in the PDOS of the surface layer (Blue line, in the area of energy lower than HOMO) and the contribution of Al atoms is included in the PDOS of the surface layer (Blue line, in the area of energy larger than LUMO).

For the sextet state the theoretical band gap is 3.67 eV for α-spin component. The gap is mainly determined by the energy level difference between the

electron-filled p orbitals of the O atoms (with moderate contributions from Fe_{III}, see HOMO in SI) and the unfilled orbitals of Al atoms. The band gap of 3.70 eV of the Fe_{III} substituted system is reasonably close to the gap of 3.90 eV of the (110) surface of pure alumina. It is the moderate contributions of the d orbitals from Fe_{III} that causes the small reduction of the band gap. For β-spin component, the predicted band gap is 1.50 eV. The gap is managed by the energy difference between the filled orbitals of O's and the empty d orbitals of Fe_{III} for the β-spin. Low energy electron transition is likely to take place from O to Fe_{III} on the (110) surface layer.

Concluding remarks

Examination of the stable (110) surface of γ-alumina reveals that there are one tri-coordinated Al and three tetra-coordinated Al sites on the surface. These sites can be classified as three different types. With the carefully calibrated density functional approach (M12-L/SV), three types of Fe single site substitutions on the (110) surface of γ-alumina have been investigated under the periodic boundary conditions. The most stable Fe replacement site on the (110) surface of γ-alumina has been found to be the tri-coordinated Fe_I position. The quartet spin state is the ground state for the Fe replacements on the tri-coordinated Al_I and the tetra-coordinated Al_{II} sites on (110) surface of γ-Al_2O_3. However, the energy

differences between the doublet and quartet are small, approximately 2~5 kcal/mol, for both sites. Thus, the doublet state of Fe_I and Fe_{II} substituted (110) surface of γ-Al_2O_3 should not be overlooked. Fe_{III} replacement leads to the doublet as the ground state. Also, its low energy excited state (quartet) should be as important since the transition energy is only about 7 kcal/mol.

In general, substitution of Al by Fe atom on (110) surface leads to elongations of metal—O distances, especially with the O atoms from the sub-layer. The replacement of Fe on Al site leads to charge redistributions of the neighboring O atoms, causing less negative charged O's to be located around the Fe. However, sublayer charge distribution is less affected by the Fe substitution on (110) surface as compared to the surface layer for the ground state. Similar charge variation trend can also be identified for the excited states.

The significant contribution of p orbital of the O atom on the surface phase to the LUMO has been revealed for the tri-coordinated Fe_I substitution on (110) surface. The corresponding oxygen atoms (O_A and O_A1) have been activated due to the existence of Fe_I in their neighborhood. The loosened neighboring Al_{III}—O_A bonds match this activation. This activation of O might be an important source of the reactive O during the Fe catalytic oxidation of CO.

In the sextet states, for all three types of substitution sites the band gap is controlled by the occupied p orbitals of O atoms and the unoccupied d orbitals of Fe. Low energy electron excitations are expected to induce electron transfer from the surface oxygen to the substituted Fe on the (110) surface of γ-Al_2O_3.It causes

reduction of Fe on the surface.

Acknowledgments

Work in the USA was supported by the ONR grant N00014171306. The computation time was provided by the Extreme Science and Engineering Discovery Environment (XSEDE) by National Science Foundation Grant Number OCI-1053575 and XSEDE award allocation Number DMR110088 and by the Mississippi Center for Supercomputer Research.

References

1. Lichen Liu, L.; Corma, A. Metal Catalysts for Heterogeneous Catalysis: From Single Atoms to Nanoclusters and Nanoparticles. *Chem. Rev*. **2018**, 118, 4981−5079.

2. Maldonado, C. S.; De la Rosa, J. R.; Lucio-Ortiz, C. J.; Hernández-Ramírez, A.; Barraza, F. F. C.; Valente, J. S. Low Concentration Fe-Doped Alumina Catalysts Using Sol-Gel and Impregnation Methods: The Synthesis, Characterization and Catalytic Performance during the Combustion of Trichloroethylene. *Materials* **2014**, 7, 2062-2086.

3. Mosallanejad, S.; Dlugogorski, B. Z.; Kennedy, E. M.; Stockenhuber, M. On the Chemistry of Iron Oxide Supported on γ-Alumina and Silica Catalysts. *ACS Omega* **2018**, 3, 5362−5374.

4. Yang, T.; Fukuda, R.; Hosokawa, S.; Tanaka, T.; Sakaki, S.; Ehara. M. A Theoretical Investigation on CO Oxidation by Single-Atom Catalysts M1/γ-Al_2O_3 (M=Pd, Fe, Co, and Ni). *ChemCatChem* **2017**, 9, 1222 – 1229.

5. Fu, Q.; Li, W.-X.; Yao, Y.; Liu, H.; Su, H.-Y.; Ma, D.; Gu, X.-K.; Chen, L.; Wang, Z.; Zhang, H.; Wang, B.; Bao, X. Interface-Confined Ferrous Centers for Catalytic Oxidation. *Science* **2010**, 328, 1141-1144.

6. Haruta, M. Size- and Support-Dependency in the Catalysis of Gold. *Catal. Today* **1997**, 36, 153−166.

7. Qiao, B.; Liang, J.-X.; Wang, A.; Xu, C.-Q.; Li, J.; Zhang, T.; Liu, J. J. Ultrastable Single-Atom Gold Catalysts with Strong Covalent Metal- Support Interaction (CMSI). *Nano Res*. **2015**, 8, 2913–2924.

8. Qiao, B.; Liu, J.; Wang, Y.-G.; Lin, Q.; Liu, X.; Wang, A.; Li, J.; Zhang, T.; Liu, J. Highly Efficient Catalysis of Preferential Oxidation of CO in H -Rich Stream by Gold Single-Atom Catalysts. *ACS Catal*. **2015**, 25, 6249–6254.

9. Qiao, B.; Wang, A.; Yang, X.; Allard, L. F.; Jiang, Z.; Cui, Y.; Liu, J.; Li, J.; Zhang, T. Single-Atom Catalysis of CO Oxidation Using Pt_1/ FeOx. *Nat*. *Chem*. 2011, 3, 634–641.

10. Moses-DeBusk, M.; Yoon, M.; Allard, L. F.; Mullins, D. R.; Wu, Z.; Yang, X.; Veith, G.; Stocks, G. M.; Narula, C. K. CO oxidation on Supported Single Pt Atoms: Experimental and ab initio Density Functional Studies of CO Interaction with Pt Atom on θ-Al_2O_3(010) Surface. *J*. *Am*. *Chem*. *Soc*. 2013, 135, 12634–12645.

11. DeRita, L.; Dai, S.; Lopez-Zepeda, K.; Pham, N.; Graham, G. W.; Pan, X.; Christopher, P. Catalyst Architecture for Stable Single Atom Dispersion Enables Site-Specific Spectroscopic and Reactivity Measure- ments of CO Adsorbed to Pt Atoms, Oxidized Pt Clusters, and Metallic Pt Clusters on TiO_2. *J*. *Am*. *Chem*. *Soc*. **2017**, 139, 14150–14165.

12. Kistler, J. D.; Chotigkrai, N.; Xu, P.; Enderle, B.; Praserthdam, P.; Chen, C. Y.; Browning, N. D.; Gates, B. C. A Single-Site Platinum CO Oxidation Catalyst in Zeolite KLTL: Microscopic and Spectroscopic Determination of the Locations of the Platinum atoms. *Angew*. *Chem*., *Int*. *Ed*. **2014**, 53, 8904–8907.

13. Saavedra, J.; Whittaker, T.; Chen, Z.; Pursell, C. J.; Rioux, R. M.; Chandler, B. D. Controlling Activity and Selectivity Using Water in the Au-Catalysed Preferential Oxidation of CO in H_2. *Nat*. *Chem*. **2016**, 8, 584–589.

14. Jones, J.; Xiong, H.; DeLaRiva, A. T.; Peterson, E. J.; Pham, H.; Challa, S. R.; Qi, G.; Oh, S.; Wiebenga, M. H.; Pereira Hernandez, X. I.; Wang, Y.; Datye, A. K. Thermally stable single-atom platinum-on-ceria catalysts via atom trapping. *Science* **2016**, 353, 150–154.

15. Zhang, Z.; Zhu, Y.; Asakura, H.; Zhang, B.; Zhang, J.; Zhou, M.; Han, Y.; Tanaka, T.; Wang, A.; Zhang, T.; et al. Thermally Stable Single Atom Pt/m-Al_2O_3 for Selective Hydrogenation and CO Oxidation. *Nat*. *Commun*. **2017**, 8, 16100.

16. Peterson, E. J.; DeLaRiva, A. T.; Lin, S.; Johnson, R. S.; Guo, H.; Miller, J. T.; Hun Kwak, J.; Peden, C. H.; Kiefer, B.; Allard, L. F.; Ribeiro, F. H.; Datye, A. K. Low-temperature Carbon Monoxide Oxidation Catalysed by Regenerable Atomically Dispersed Palladium on Alumina. *Nat*. *Commun*. **2014**, 5, 4885.

17. Gu, X.-K.; Qiao, B.; Huang, C.-Q.; Ding, W.-C.; Sun, K.; Zhan, E.;Zhang,T.;Liu,J.;Li,W.-X.SupportedSinglePt_1/Au_1Atomsfor Methanol Steam Reforming. *ACS Catal*. **2014**, 4, 3886–3890.

18. Zhu, Y.; An, Z.; He, J. Single-Atom and Small-Cluster Pt Induced by Sn (IV) sites Confined in an LDH Lattice for Catalytic Reforming. *J. Catal*. **2016**, 341, 44–54.

19. De, S.; Saha, B.; Luque, R. Hydrodeoxygenation Processes: Advances on Catalytic Transformations of Biomass-Derived Platform Chemicals into Hydrocarbon Fuels. *Bioresour. Technol*. **2015**, 178, 108– 118.

20. Guo, X.; Fang, G.; Li, G.; Ma, H.; Fan, H.; Yu, L.; Ma, C.; Wu, X.; Deng, D.; Wei, M.; et al. Direct, Nonoxidative Conversion of Methane to Ethylene, Aromatics, and Hydrogen. *Science* **2014**, 344, 616–619.

21. Duan, H.; Li, M.; Zhang, G.; Gallagher, J. R.; Huang, Z.; Sun, Y.; Luo, Z.; Chen, H.; Miller, J. T.; Zou, R.; et al. Single-Site Palladium(II) Catalyst for Oxidative Heck Reaction: Catalytic Performance and Kinetic Investigations. *ACS Catal*. **2015**, 5, 3752–3759.

22. Metzger, E. D.; Brozek, C. K.; Comito, R. J.; Dinca˘, M. Selective Dimerization of Ethylene to 1-Butene with a Porous Catalyst. *ACS Cent. Sci*. **2016**, 2, 148–153.

23. Zhang, S.; Nguyen, L.; Liang, J.-X.; Shan, J.; Liu, J.; Frenkel, A. I.; Patlolla, A.; Huang, W.; Li, J.; Tao, F. Catalysis on Singly Dispersed Bimetallic Sites. *Nat. Commun*. **2015**, 6, 7938.

24. Nguyen, L.; Zhang, S.; Wang, L.; Li, Y.; Yoshida, H.; Patlolla, A.; Takeda, S.; Frenkel, A. I.; Tao, F. Reduction of Nitric Oxide with Hydrogen on Catalysts of Singly Dispersed Bimetallic Sites Pt_1Co_m and Pd_1Co_n. *ACS Catal*. **2016**, 6, 840–850.

25. Han, Y.; Wang, Y.-G.; Chen, W.; Xu, R.; Zheng, L. R.; Zhang, J.; Luo, J.; Shen, R.-A.; Zhu, Y.; Cheong, W.-C.; et al. Hollow N-doped Carbon Spheres with Isolated Cobalt Single Atomic Sites: Superior Electrocatalysts for Oxygen Reduction. *J. Am. Chem. Soc*. **2017**, 139, 17269–17272.

26. Yin, P.; Yao, T.; Wu, Y.; Zheng, L.; Lin, Y.; Liu, W.; Ju, H.; Zhu, J.; Hong, X.; Deng, Z.; et al. Single Cobalt Atoms with Precise N- Coordination as Superior Oxygen Reduction Reaction Catalysts. *Angew. Chem., Int. Ed*. **2016**, 55, 10800–10805.

27. Cheng, Q.; Yang, L.; Zou,L.; Zou, Z.; Chen, C.; Hu, Z.; Yang, H. Single Cobalt Atom and N Codoped Carbon Nanofibers as Highly Durable Electrocatalyst for Oxygen Reduction Reaction. *ACS Catal*. **2017**, 7, 6864–6871.

28. Zheng, Y.; Jiao, Y.; Zhu, Y.; Cai, Q.; Vasileff, A.; Li, L. H.; Han, Y.; Chen, Y.; Qiao, S. Z. Molecule-Level g-C_3N_4 Coordinated Transition Metals as a New Class of Electrocatalysts for Oxygen Electrode Reactions. *J. Am. Chem. Soc.* **2017**, 139, 3336–3339.

29. Chen, Y.; Ji, S.; Wang, Y.; Dong, J.; Chen, W.; Li, Z.; Shen, R.; Zheng, L.; Zhuang, Z.; Wang, D.; et al. Isolated Single Iron Atoms Anchored on N-Doped Porous Carbon as an Efficient Electrocatalyst for the Oxygen Reduction Reaction. *Angew. Chem., Int. Ed.* **2017**, 56, 6937– 6941.

30. Chung, H. T.; Cullen, D. A.; Higgins, D.; Sneed, B. T.; Holby, E. F.; More, K. L.; Zelenay, P. Direct Atomic-Level Insight Into the Active Sites of a High-Performance PGM-free ORR Catalyst. *Science* **2017**, 357, 479–484.

31. Zhu, C.; Fu, S.; Song, J.; Shi, Q.; Su, D.; Engelhard, M. H.; Li, X.; Xiao, D.; Li, D.; Estevez, L. Self-Assembled Fe-N-Doped Carbon Nanotube Aerogels with Single-Atom Catalyst Feature as High- Efficiency Oxygen Reduction Electrocatalysts. *Small* **2017**, 13, 1603407.

32. Zhang, Z.; Gao, X.; Dou, M.; Ji, J.; Wang, F. Biomass Derived N-Doped Porous Carbon Supported Single Fe Atoms as Superior Electrocatalysts for Oxygen Reduction. *Small* **2017**, 13, 1604290.

33. Wisechert, R.; Florian, P.; Copéret, C.; Massiot, D.; Sautet, P. Visibility of Al Surface Sites of γ-Alumina: A Combined Computational and Experimental Point of View. *J. Phys. Chem. C* **2014**, *118*, 15292-15299.

34. Kwak, J. H.; Mei, D.; Peden, C. H. F.; Rousseau, R.; Szanyi, J. (100) Facets of γ-Al_2O_3: The Active Surfaces for Alcohol Dehydration Reactions. Catal. Lett. 2011, 141, 649–655.

35. Kwak, J. H.; Hu, J.; Mei, D.; Yi, C.-W.; Kim, D. H.; Peden, C. H. F.; Allard, L. F.; Szanyi, J. Coordinatively Unsaturated Al^{3+} Centers as Binding Sites for Active Catalyst Phases of Platinum on γ- Al_2O_3. *Science* **2009**, 325, 1670–1673.

36. Copeland, J. R.; Shi, X.-R.; Sholl, D. S.; Sievers, C. Surface Interactions of C_2 and C_3 Polyols with γ-Al_2O_3 and the Role of Co-adsorbed Water. *Langmuir* **2012**, *29*, 581–593.

37. Wilson, S. J. The dehydration of boehmite, γ-AlOOH, to γ-Al_2O_3. *J. Solid State Chem.* **1979**, *30,* 247-255.

38. Goswami, R.; Pande, C. S.; Bernstein, N.; Johannes, M. D.; Baker, C.; Villalobos, G. A high degree of enhancement of strength of sputter deposited Al/Al_2O_3 multilayers upon post annealing. *Acta Materialia* **2015**, *95*, 378-385.

39. Digne, M.; Sautet, P.; Raybaud, P.; Euzen, P.; Toulhoat, H. Use of DFT to achieve a rational understanding of acid–basic properties of γ-alumina surfaces. *J. Catalys*. **2004**, *226*, 54-68.

40. Digne, M.; Sautet, P.; Raybaud, P.; Euzen, P.; Toulhoat, H. Hydroxyl Groups on γ-Alumina Surfaces: A DFT Study. *J. Catalys*.**2002**, *211*, 1-5.

41. Pinto, H. P.; Nieminen, R. M.; Elliott, S. D. *Ab initio* study of γ−Al2O3 surfaces. *Phys. Rev. B* **2004**, *70*, 125402.

42. Kovarik, L.; Genc, A.; Wang, C.; Qiu, A.; Peden, C. H. F.; Szanyi, J.; Kwak, J. H. Tomography and High-Resolution Electron Microscopy Study of Surfaces and Porosity in a Plate-like γ-Al_2O_3. *J. Phys. Chem. C* 2013, *117*, 179-186.

43. Wisechert, R.; Copéret, C.; Delbecq, F.; Sautet, P. Optimal Water Coverage on Alumina: A Key to Generate Lewis Acid–Base Pairs that are Reactive Towards the C—H Bond Activation of Methane. *Angew. Chem. Int. Ed*. **2011**, *50*, 3202-3205.

44. Larson, J. G.; Hall, W. K. Studies of the Hydrogen Held by Solids. VII. The Exchange of the Hydroxyl Groups of Alumina and Silica-Alumina Catalysts with Deuterated Methane. *J. Phys. Chem.* **1965**, *69*, 3080-3089.

45. Robertson, P. J.; Scurrell, M. S.; Kemball, C. Exchange of alkanes with deuterium over γ-alumina. A Brønsted linear free energy relationship. *J. Chem. Soc. Faraday Trans. 1* **1975**, *71*, 903-912.

46. Hargreaves, J. S. J.; Hutchings, G. J.; Joyner, R. W.; Taylor, S. H. A study of the methane–deuterium exchange reaction over a range of metal oxides. *Appl. Actal. A* **2002**, *227*, 191-200.

47. Quanzhi, L.; Amenomiya, Y. Exchange reaction of methane on some oxide catalysts. *Appl. Catal.* **1986**, *23*, 173-182.

48. Knozinger, H.; Ratnasamy, P. Catalytic Aluminas: Surface Models and Characterization of Surface Sites. *Catal. Rev. Sci. Eng.* **1978**, *17*, 31-70.

49. Joubert, J.; Salameh, A.; Krakoviack, V.; Delbecq, F.; Sautet, P.; Coperet, C.; Basset, J. –M. Heterolytic Splitting of H_2 and CH_4 on γ-Alumina as a Structural Probe for Defect Sites. *J. Phys. Chem. B* **2006**, *110*, 23944-23950.

50. Gu, J.; Wang, J.; Leszczynski, J. Structure and Energetics of (111) Surface of γ-Al2O3: Insights from DFT Including Periodic Boundary Approach *ACS Omega*, **2018**, 3, 1881−1888.

51. Gu, J.; Wang, J.; Leszczynski, J. Single Fe Site on the Surface of γ-Al_2O_3: Insights from Density Functional Theory Periodic Boundary Approach *J. Phys. Chem. C* **2020**, *124*, 20931-20941.

52. Peverati, R.; Truhlar, D. G. An improved and broadly accurate local approximation to the exchange–correlation density functional: The MN12-L functional for electronic structure calculations in chemistry and physics. *Phys. Chem. Chem. Phys.* **2012***, 10,* 13171-13174.

53. Kresse, G.; Joubert, D. From ultrasoft pseudopotentials to the projector augmented-wave method. *Phys. Rev. B* **1999,** *59*, 1758-1775.

54. Kresse, G.; Furthmüller, J. Efficient iterative schemes for *ab initio* total-energy calculations using a plane-wave basis set. *Phys. Rev. B* **1996,** *54*, 11169-11186.

55. Schaefer, A.; Horn, H.; Ahlrichs, R. Fully optimized contracted Gaussian-basis sets for atoms Li to Kr *J. Chem. Phys*. **1992**, *97*, 2571-2577.

56. Gaussian 09, Revision D**.01**, Frisch, M. J.; Trucks, G. W.; Schlegel, H. B.; Scuseria, M. A.; Robb, J. R.; Cheeseman, G.; Scalmani, V.; Barone, B.; Mennucci, G. A.; Petersson, G. E. et al. Gaussian, Inc., Wallingford CT, 2009.